THE ROYAL SOCIETY

J. R. Soc. Interface (2004) **1**, 91–97
DOI: 10.1098/rsif.2004.0010

Linearity and time-scale invariance of the creep function in living cells

Guillaume Lenormand†, Emil Millet, Ben Fabry, James P. Butler and Jeffrey J. Fredberg

Physiology Program, School of Public Health, Harvard University, 665 Huntington Avenue, Boston, MA, 02115, USA

We report here the creep function measured in three cell types, after a variety of interventions, and over three time decades (from 3 ms to 3.2 s). In each case the response conformed to a power law, implying that no distinct molecular relaxation times or time constants could characterize the response. These results add to a growing body of evidence that stands in contrast to widely used viscoelastic models featuring at most a few time constants. We show instead that the ability of the matrix to deform is time-scale invariant and characterized by only one parameter: the power law exponent that controls the transition between solid-like and liquid-like behaviour. Moreover, we validate linearity by comparison of measurements in the time and frequency domains.

Keywords: magnetic twisting cytometry; creep compliance; cell mechanics; elasticity; soft glassy rheology

1. INTRODUCTION

Cell mechanics has been studied using a variety of techniques over the past 50 years, among which are atomic force microscopy (Wu *et al.* 1998), cell indentation (Koay *et al.* 2003), magnetocytometry (Butler & Kelly 1998; Crick & Hughes 1950; Karcher *et al.* 2003; Laurent *et al.* 2002*a*; Wang *et al.* 1993), micropipette aspiration (Chien & Sung 1984; Evans & Yeung 1989; Yeung & Evans 1989), micro plates (Thoumine & Ott 1997), optical tweezers (Laurent *et al.* 2002*b*) and magnetic tweezers (Bausch *et al.* 1998, 1999; Ziemann *et al.* 1994). Based on such observations, cell rheology has usually been described using viscoelastic models characterized by a small number of distinct relaxation times. Commonly, those relaxation times have been interpreted in terms of viscosity and elasticity of cortical (Evans & Yeung 1989; Karcher *et al.* 2003; Laurent *et al.* 2002*a*; Yeung & Evans 1989) and/or cytoplasmic structures (Bausch *et al.* 1998, 1999; Butler & Kelly 1998; Chien & Sung 1984; Crick & Hughes 1950; Evans & Yeung 1989; Karcher *et al.* 2003; Koay *et al.* 2003; Laurent *et al.* 2002*a*,*b*; Thoumine & Ott 1997; Wang *et al.* 1993; Wu *et al.* 1998; Yeung & Evans 1989; Ziemann *et al.* 1994). These models predict that the creep function (i.e. the ongoing deformation in response to a step stress) should exhibit two or three distinct regimes (Findley *et al.* 1976): an initial instantaneous elasticity followed by an exponential approach to a steady state, leading finally to a viscous flow at longer times.

The dynamic responses reported here add to a growing body of evidence that stands in contrast to those predictions (Lau *et al.* 2003; Yamada *et al.* 2000; Yanai *et al.* 2004). We have measured the creep function over three decades in time (from 3 ms to 3.2 s, a range substantially wider than those previously reported), in three different cell types, and with a variety of experimental interventions. In every case a power law response prevailed, implying that within the cell body, relaxations at all time scales were present simultaneously; no distinct relaxation time stood out, and no distinct molecular relaxation time or time constant could characterize the response. Of course, models with a multitude of distinct relaxation time scales cannot be ruled out, but we address here the alternative hypothesis that another type of process might account for these observations.

2. MATERIALS AND METHODS

2.1. Probing cell mechanics

The complex elastic modulus and the creep function of human airway smooth muscle (HASM) cells, human fetal lung (HFL) fibroblasts and rat airway smooth muscle (RASM) cells were measured using an optical magnetic twisting cytometer (OMTC) (Fabry *et al.* 2001, 2003). Briefly, ferrimagnetic beads (4.2 μm in diameter) were incubated on cells for 20 min at 37 °C. Beads had been coated with a peptide containing the sequence RGD (Arg-Gly-Asp) allowing them to attach specifically to integrin receptors and were used to probe CSK mechanics deep in the cell interior (Fabry *et al.* 2001, 2003; Hu *et al.* 2003). A pair of magnetizing coils and a pair of twisting coils were mounted on the stage of an inverted microscope. The beads were first magnetized horizontally by a magnetic field pulse

†Author for correspondence (glenorma@hsph.harvard.edu).

Received 12 May 2004
Accepted 14 September 2004
Published online 1 October 2004

($\sim$0.1 T for 0.1 ms) using the magnetizing coils (figure 1*a*). A vertical magnetic field H applied by the twisting coils induced a mechanical torque on each bead and caused both a rotation and a lateral displacement of the beads (Mijailovich *et al.* 2002). The mechanical torque T per bead volume was $T = cH\cos\theta$, where c equals 2.1 Pa Gauss^{-1} and θ is the bead's rotation. In any given cell well, the individual displacements of $\sim$100 beads on $\sim$100 cells were recorded simultaneously from CCD camera images using an intensity-weighted centre-of-mass algorithm. The accuracy in the bead position was 10 nm; the exposure time was 0.1 ms. Two kinds of forcing were applied: sinusoidal oscillations and step torques.

2.2. Measuring the complex elastic modulus

Sinusoidal forcing was used to measure a storage modulus $g'(f)$ and a loss modulus $g''(f)$ over four decades in frequency f (from 0.1 Hz to 1 kHz). This complex elastic modulus of the cell was defined by $g(f) = \tilde{T}(f)/\tilde{d}(f)$, where $\tilde{T}$ is the Fourier transform of the mechanical torque per bead volume (Pa s) and $\tilde{d}$ the Fourier transform of the resulting bead displacements (nm s); $g(f) = g'(f) + ig''(f)$. This elastic modulus has dimensions of Pa nm^{-1} and could be transformed to the conventional complex elastic modulus $G(f)$ (with units of Pa), using a geometric factor α; $G(f) = \alpha g(f)$. The geometric factor α has been evaluated using a finite-element model of cell deformation (Mijailovich *et al.* 2002), and depends mainly on the cell height and on the degree of bead embedding. Assuming 10% of the bead diameter embedded in a cell 5 µm high sets α to 6.8 µm. It is thus possible using OMTC measurements to evaluate the conventional complex elastic modulus.

2.3. Measuring the creep function

A step torque was used to measure the creep function. Assuming system linearity (as established experimentally below), the Boltzmann superposition principle gives the strain $\varepsilon(t)$ measured during a creep test at time t (Findley *et al.* 1976) as

$$\varepsilon(t) = \int_0^t J(t-\xi)\frac{\partial\sigma(\xi)}{\partial\xi}\,\mathrm{d}\xi,$$

where $\sigma(t)$ is the applied stress. The creep function $J(t)$ describes the dependence of strain upon stress history. In our experiments, we defined a related creep function as $j(t) = d(t)/T_0$ with $d(t)$ being the lateral bead displacement and T_0 being the applied torque per unit bead volume. This creep function has dimensions of nm Pa^{-1} and can be transformed to the conventional creep function $J(t)$ (with units of Pa^{-1}) by the same geometric factor α through the relationship $J(t) = j(t)/\alpha$. This geometric factor need serve only as a rough approximation however, because it cancels out in the scaling procedure described below, which is model-independent.

To measure the creep function, a constant magnetic field of 20 Gauss ($T_0 = 42$ Pa) was applied for 3.2 s causing the beads to rotate and translate, followed by a recovery period of 9.6 s ($T_0 = 0$ Pa) causing a partial return of beads to their initial positions (figure 1*b*). To ensure a horizontal magnetization of the beads for the following cycle, the beads were re-magnetized 1.5 s before applying each torque step. This 12.8 s cycle was repeated 10 times for every measurement of the creep function. We analysed the last five cycles of this sequence in order to have cycles with similar deformation history. Heterodyning was used to probe small times by triggering the first image of each cycle at different times (figure 1*b*).

Because the torque decreases as the bead rotates, the applied torque was nearly, but not perfectly, constant over the course of the creep measurement. Mijailovich *et al.* (2002) have used a finite element analysis to compute the relation between the bead displacement and its rotation. For 90% of the beads, the torque decreases by less than 3% and was thus considered constant.

2.4. Methodological limitations

Limitations and artifacts associated with magnetic bead twisting have been reported in detail elsewhere (Fabry *et al.* 2003; Mijailovich *et al.* 2002; Puig-De-Morales *et al.* 2004). Among these limitations are that the interaction of the magnetic microbead with the cell induces local remodelling events that alter the structure that is being probed, the geometry of the bead–cell interaction is also not controlled, and a length scale α (described above) must be invoked in order to convert raw data into a proper elastic modulus.

These limitations are counterbalanced in many applications by the unique capabilities of the approach. Principal strengths include the fact that the bead can apply a mechanical load to the cell body in the physiologic range of stress (from below 1 Pa to over 100 Pa); these loads are transmitted to the cell body via specific receptor-ligand systems selectable by the bead coating (Puig-De-Morales *et al.* 2004). Dynamic responses can be measured at frequencies as high as 1 kHz, and even at the highest frequencies studied, inertia does not come into play and the viscous loads associated with the supernatant are smaller than the loads associated with the cell by several orders of magnitude (Fabry *et al.* 2001, 2003). Many beads can be tracked simultaneously using OMTC and data from hundreds or even thousands of cells can be collected with high fidelity in a relatively short time. Importantly, cells probed with this technology display mechanical responsiveness that is consistent with physiologic responses measured at the tissue and organ level (An *et al.* 2002; Hubmayr *et al.* 1996). Moreover, dynamic moduli measured with this approach are consistent with measurements in the same cells made with independent methods such as atomic force microspcopy (Alcaraz *et al.* 2003).

3. RESULTS AND DISCUSSION

3.1. Power law behaviour

We first measured the creep function under baseline conditions. Figure 1*b* shows median values of bead displacement versus time on HASM cells for five cycles.

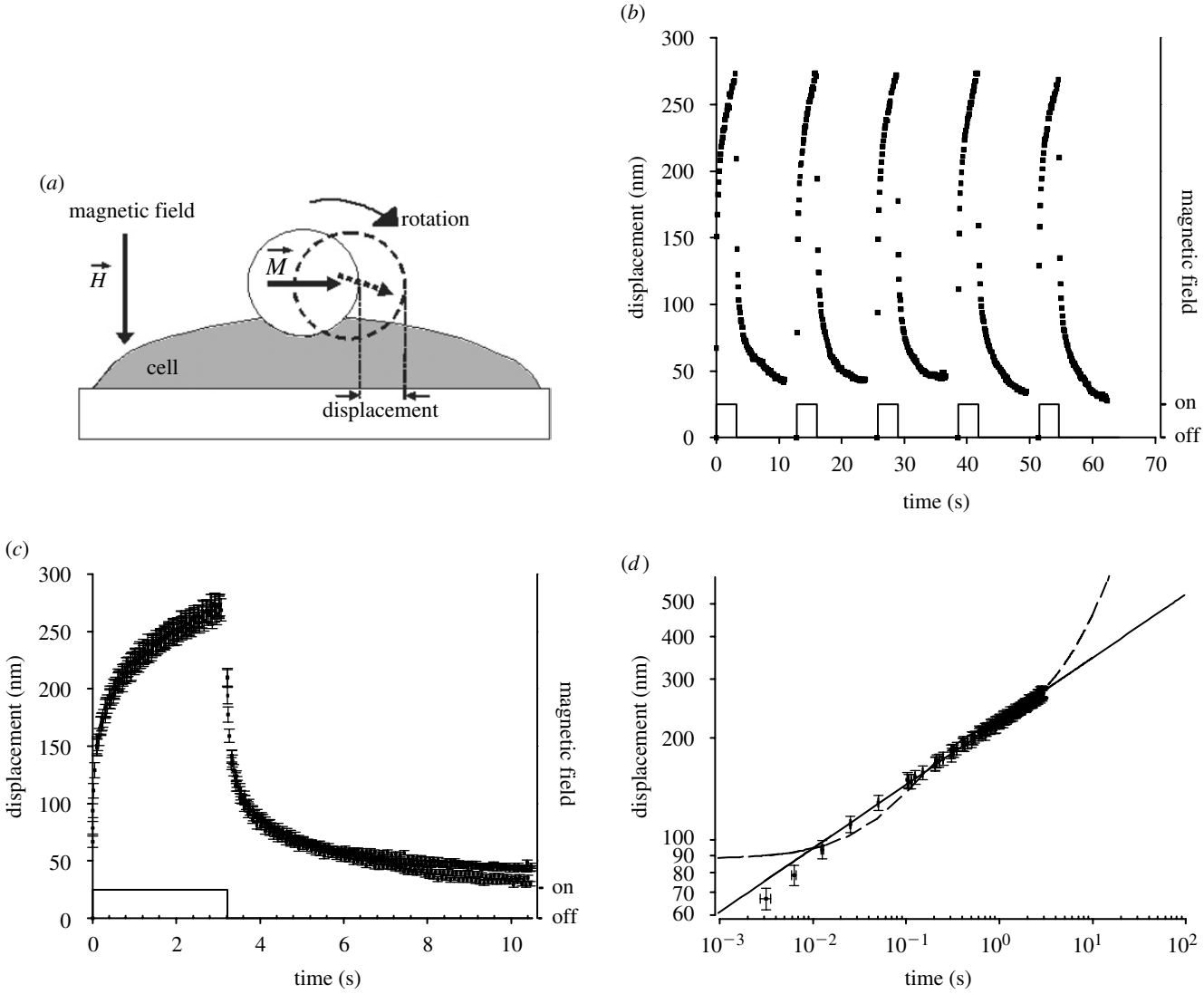

Figure 1. Lateral bead displacement versus time for step changes in applied torque (median ± standard error) on HASM cells. (*a*) The magnetic field causes both a rotation and a displacement of the bead. (*b*) Median values of displacement ($n = 903$ beads) and torque versus time. (*c*) The five cycles are superposed. The shape of the curve is similar to that reported by others (Bausch *et al.* 1998, 1999; Ziemann *et al.* 1994). (*d*) Displacement on a log–log scale. Best fit by a Burgers viscoelastic model (dashed line) and power law (solid line; power law exponent 0.178). Burgers model (which has four free parameters) show a clear departure between data and fit at small times. These two models make very different predictions outside the measurement range. The small discrepancy between data and power law fit at small time is consistent with the small Newtonian viscosity μ (see text).

Because no systematic trend was noticed from cycle to cycle, we superposed the five cycles into one (figure 1*c*). On a log–log scale (figure 1*d*) the displacement of beads over three time decades increased according to a weak power law ($d(t) = 293t^{0.178}$) with a correlation coefficient r^2 of 0.992. The creep function corresponds to this same curve divided by the applied torque T_0. Importantly, the power law responses persisted on a bead-by-bead basis; thus the multiplicity of time scales associated with power law behaviour cannot be attributable to population averages that pool together data sampled from many different individual cells or different cell regions.

Cells were also challenged with histamine (a contractile agonist), N6,2-O-dibutyryladenosine 3,5-cyclic monophosphate (DBcAMP, a relaxing agonist) and cytochalasin D (cytoD, causing the disruption of actin filaments). In each case, creep functions (figure 2) conformed to power law behaviour. The four curves were well-fitted by $j_c = A_c(t/t_0)^{x_c-1}$ (model 1), with $t_0 = 1\,\mathrm{s}$ and where the subscript c stands for each of the challenges; r^2 was equal to 0.995 (Table 1). Histamine caused the creep function to decrease, i.e. the stiffness increased and the power law exponent fell slightly. In contrast, ablating baseline contractile tone with DBcAMP caused $j(t)$ to increase, i.e. the stiffness decreased and the power law exponent increased. When actin filaments were disrupted with cytochalasin D, $j(t)$ increased even more and the exponent increased further. The changes in the power law exponent, and in the prefactor A_c were statistically significant (using a z-test, $p < 0.001$).

Table 1. Comparison between model 1 and model 2 on HASM cells. Model 1 corresponds to independent power laws ($j_c(t) = A_c(t/t_0)^{x_c-1}$ with $t_0 = 1\,s$); model 2 has a common intersection ($j_c(t) = J_0(t/\tau_0)^{x_c-1}$, equation (3.2)). SS: sum of squared residuals. The values in parentheses are given to compare the two models. Values are median ± standard deviation.

	Model 1	Model 2
x_{baseline}	1.209 ± 0.003	1.198 ± 0.002
$x_{\text{histamine}}$	1.180 ± 0.003	1.188 ± 0.002
x_{DBcAMP}	1.219 ± 0.003	1.217 ± 0.002
x_{CytoD}	1.223 ± 0.003	1.227 ± 0.002
A_{baseline} (nm Pa^{-1})	2.712 ± 0.008	(2.716)
$A_{\text{histamine}}$ (nm Pa^{-1})	1.991 ± 0.006	(1.989)
A_{DbcAMP} (nm Pa^{-1})	5.035 ± 0.015	(5.036)
A_{CytoD} (nm Pa^{-1})	6.772 ± 0.020	(6.770)
J_0 (nm Pa^{-1})	—	0.005 [0.003 − 0.008]
τ_0 (s)	—	1.3×10^{-14} [$7.7 \times 10^{-16} - 2 \times 10^{-13}$]
r^2	0.9953	0.9951
SS	0.8523	0.8958

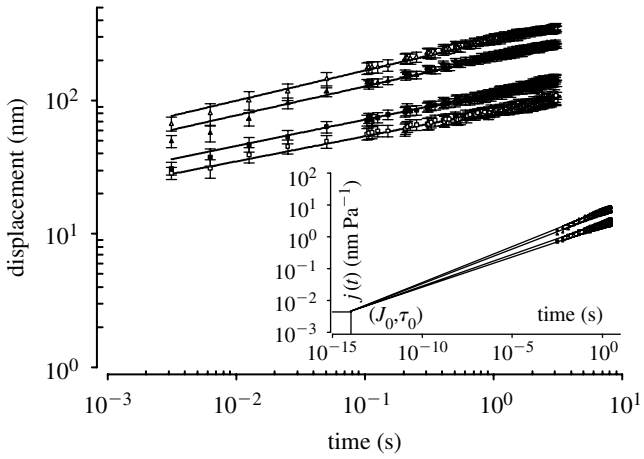

Figure 2. Median values (± standard error) of bead displacement on HASM cells under baseline condition (■, $n = 793$ beads; power law exponent 0.198), and after 10 minutes treatment with 10^{-4} M histamine (□, $n = 1337$ beads; power law exponent 0.188); 15 minutes with 10^{-3} M DBcAMP (△, $n = 1385$ beads; power law exponent 0.217) and 30 minutes with 2×10^{-6} M cytoD (▲, $n = 713$ beads; power law exponent 0.227). The inset shows the creep function and the best fit by model 2, defining a common intersection at small time. The power law exponents above are given for model 2.

3.2. Linearity

We assessed linearity in two ways. First, we measured the displacement of beads at 1 s versus the applied torque and observed a linear relation for torques between 5 Pa and 100 Pa, implying linear mechanical behaviour in that range (data not shown). In addition, active stiffening or reinforcement responses of the cell were not evident in the range of torques reported here.

Second, we evaluated the validity of the superposition principle by comparing measurements in the time domain versus frequency domain on the same cells. As reported previously (Fabry *et al.* 2001, 2003), the storage modulus g' was well fitted by a power law over four frequency decades. The loss modulus g'' followed a power law with the same exponent as g' at frequencies below 30 Hz and then asymptotically approached a power law with a slope of 1, which is characteristic of a Newtonian viscosity μ (with dimensions of Pa s nm^{-1}). The complex elastic modulus was well described by

$$g_c(\omega) = \frac{G_0}{\Gamma(x)} \left(\frac{i\omega}{\Phi_0}\right)^{x_c-1} + i\mu\omega, \qquad (3.1)$$

with G_0 and Φ_0 being scale factors for stiffness and frequency, Γ being the gamma function and $\omega = 2\pi f$ (Table 2). The first term on the right-hand side of (3.1), known as the structural damping law, describes a relationship between the exponent of the power law $(x - 1)$ and the transition from Hookean solid-like ($x = 1$) to Newtonian liquid-like ($x = 2$) behaviour. The formulation of (3.1) is essentially equivalent to that of Fabry *et al.* (2001, 2003).

For linear materials, (3.1) describing the complex modulus and (3.2) describing the creep function (see below), comprise identical laws if G_0 and Φ_0 are identified as $1/J_0$ and $1/\tau_0$ respectively (Findley *et al.* 1976). The agreement between the time-domain and the frequency-domain data was very good (Table 2), although the model for the creep function we used did not include the small Newtonian viscosity. Indeed, the data at small times fell by a small but systematic amount below the fitting line (figures 1*d* and 2), which was quantitatively consistent with the contribution of this Newtonian viscous term. This follows from the evaluation using Mittag–Leffler functions (Erdélyi *et al.* 1954) of $j(t) = \mathcal{L}^{-1}[1/(sg(s))]$, where $\mathcal{L}^{-1}$ denotes the inverse Laplace transform. The extrapolations to small times (figure 2 inset) did not include this additive term.

It is not at all obvious *a priori* that measurements of the creep function in the time domain versus measurements of the complex modulus in the frequency domain in living cells should be Laplace transform pairs; either nonlinearities or active mechanotransduction phenomena might have broken the principle of superposition. Data reported here establish insensitivity of the creep function to the amplitude of the forcing, and equivalence of measurements in the frequency domain versus the time domain (Fabry *et al.* 2001, 2003). Taken together, these new data represent the

Table 2. Comparison between the complex elastic modulus and the creep functions measured on the same population of HASM cells ($n > 700$ beads). Values are median ± standard deviation.

	Elastic modulus	Creep function
x_{baseline}	1.23 ± 0.01	1.245 ± 0.005
$x_{\text{histamine}}$	1.19 ± 0.01	1.211 ± 0.008
x_{DBcAMP}	1.28 ± 0.01	1.275 ± 0.008
$J_0 = 1/G_0$ (nm Pa^{-1})	0.005 [0.002 − 0.012]	0.025 [0.006 − 0.106]
$\tau_0 = 1/\Phi_0$ (s)	2.3×10^{-12} [$1 \times 10^{-14} - 4 \times 10^{-10}$]	1.2×10^{-13} [$4 \times 10^{-15} - 4 \times 10^{-11}$]
r^2	0.975	0.977

most comprehensive evidence to date establishing a linear range of cell mechanical responses.

3.3. Reduction of variables

Extrapolation of the four creep functions appeared to define a common intersection, or fixed point, at very small time (inset of figure 2). The existence of a fixed point would imply that differences in responses among the various experimental interventions could be accounted for by changes in the power law exponent only. To verify the existence of a fixed point, we analysed the data using a second model (model 2):

$$j_{\text{c}}(t) = J_0 \left(\frac{t}{\tau_0}\right)^{x_{\text{c}}-1}, \qquad (3.2)$$

where J_0 and τ_0 are scale factors that are constant for a given cell type. An analysis of variance F-test showed that model 1, which has more free parameters, fit the data significantly better. Nevertheless, models 1 and 2 gave essentially identical results (Table 1). We later adopt model 2 which fit the data as well as model 1 and did so with fewer parameters.

3.4. Universal scaling and the master curve

Creep function measurements performed on HFL fibroblasts and RASM cells were also well-fitted by (3.2), with r^2 of 0.979 and 0.997 respectively. Measurements were done under baseline conditions and after challenge with several agonists. For each measurement, we plotted the creep function $j(t)$ at 1 s (an arbitrary time) divided by the corresponding J_0 versus the parameter x. Upon doing so, all the data collapsed onto a master curve (figure 3), suggesting that although J_0 was cell-type specific, τ_0 was invariant and close to 10^{-14} s for the three cell types studied. This relationship represents a universal master curve in that a single parameter, x, defined the mechanical behaviour for a variety of cytoskeletal interventions, for three time decades, and for three different cell types.

Similar power law behaviour in the frequency domain has been reported by Fabry *et al.* (2001, 2003) (HASM cells, human bronchial epithelial cells, mouse embryonic carcinoma cells, mouse macrophages and human neutrophils) using OMTC and Alcaraz *et al.* (2003) (human alveolar and bronchial epithelial cells) using atomic force microscopy. Power law behaviours have also been reported recording spontaneous motion (Lau *et al.* 2003; Yamada *et al.* 2000) and forced motion (Yanai *et al.* 2004) of endogenous particles in the cells.

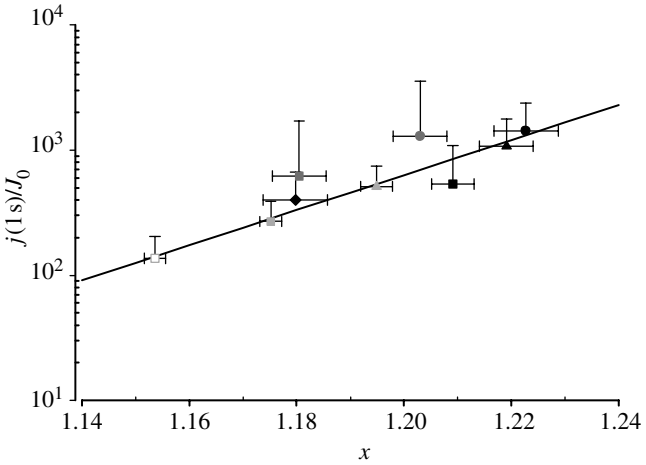

Figure 3. Master curve showing normalized bead displacement at 1 s versus x. HASM cells (black), HFL fibroblasts (grey) and RASM cells (light grey) under baseline condition (■), treatment with histamine (◇), DBcAMP (▲), cytoD (●) and 5-HT (□). The solid curve is the prediction from equation (3.2) with $\tau_0 = 10^{-14}$ s ($n > 500$ beads for each treatment.)

These data, taken together with the data reported here, suggest that power law behaviour may be a common feature of cell mechanics.

3.5. Viscoelastic models

The response curve in figure 1*c* is consistent with data reported by others (Bausch *et al.* 1998, 1999; Karcher *et al.* 2003; Koay *et al.* 2003; Ziemann *et al.* 1994) but extends those observations up to three time decades (down to a few milliseconds). Figure 1*d* shows a fit of our data with a viscoelastic Burgers model consisting of a Kelvin model and a Maxwell model in series (Findley *et al.* 1976) (essentially equivalent to that of Bausch *et al.* (1998)). The difference between the fit of the Burgers model and the fit of a power law is hardly detectable when data span only a single time decade, but over a wider time window the Burgers model is clearly unable to account for the creep response despite the fact that it has four free parameters (figure 1*d*). Accordingly, what had been interpreted previously as being an exponential response we show here to be a power law response. It might be argued that these data could be fit equally well by using a viscoelastic model comprising roughly two relaxation times per time decade, or, for our creep measurements, six free parameters in all (eight in the frequency domain). While this

is true, such an interpretation requires assignment of an *ad hoc* distribution of time constants and represents nothing more than a different parametrization of the data, albeit one requiring six free parameters (eight in the frequency domain) instead of two.

3.6. Alternative hypotheses

In some circumstances, cells need to flow like a liquid whereas in other circumstances cells have to maintain their shape and thus behave as an elastic body. The transition between liquid-like behaviour (x close to 2) and solid-like behaviour (x close to 1) is often described as a sol–gel transition, and gels near a critical gelation point do exhibit a power law behaviour similar to the one reported here (Winter & Mours 1997). As an alternative explanation, but one not mutually exclusive with the notion of critical gelation (Segre *et al.* 2001), we have suggested previously (Fabry *et al.* 2001, 2003) that cell rheology might be considered in the context of soft glassy materials (SGM). The theory of SGMs proposed in Sollich (1998) is based on a power law distribution of time constants and predicts rheological behaviour of the kind reported here (equation (3.1)). The mechanical properties of SGMs are determined principally by an effective temperature, x, which appears in the power law exponent and which Sollich interprets as the amount of jostling (i.e. molecular noise or agitation) of structural elements relative to the depth of energy wells, or cages, in which such elements are trapped.

If we apply this interpretation to the data reported here, then cell rheology could arise from cytoskeletal elements agitated and re-arranged by mutual weak interactions within their matrix. Agents that activate the contractile apparatus cause x to decrease, and the system moves toward the glass transition and a more solid-like state. Relaxing agonists and agents that disrupt the CSK cause x to increase, and the system becomes more disordered and moves towards a fluid-like state. The parameter J_0 would then be the creep function at the glass transition and the parameter τ_0^{-1} would be the maximum rate at which cytoskeletal elements rearrange.

4. CONCLUDING REMARKS

The two new results established here are comprehensive evidence of linearity of system responses and time-scale invariance of those responses. These results, which were demonstrated in three types of adherent living cells and after a variety of interventions, stand in contrast to widely used viscoelastic models with one or even several time constants. Although cell rheology shows power law responses that are known to be characteristic of soft glassy materials (Fabry *et al.* 2001, 2003), these features by themselves are not sufficient to classify these cells as soft glasses. As such, other phenomena that are considered to be the signature of glassy behaviour, especially certain types of nonlinearities, aging phenomena and the emergence of slow non-ergodic relaxation processes close to the glass transition (Fielding *et al.* 2000; Sollich 1998), become of interest.

We thank S. An and D. Tschumperlin for providing RASM cells and fibroblasts. This study was supported by HL 33009, HL/AI 65960 and HL 59682.

REFERENCES

Alcaraz, J., Buscemi, L., Grabulosa, M., Trepat, X., Fabry, B., Farre, R. & Navajas, D. 2003 Microrheology of human lung epithelial cells measured by atomic force microscopy. *Biophys. J.* **84**, 2071–2079.

An, S. S., Laudadio, R. E., Lai, J., Rogers, R. A. & Fredberg, J. J. 2002 Stiffness changes in cultured airway smooth muscle cells. *Am. J. Physiol. Cell. Physiol.* **283**, C792–C801.

Bausch, A. R., Moller, W. & Sackmann, E. 1999 Measurement of local viscoelasticity and forces in living cells by magnetic tweezers. *Biophys. J.* **76**, 573–579.

Bausch, A. R., Ziemann, F., Boulbitch, A. A., Jacobson, K. & Sackmann, E. 1998 Local measurements of viscoelastic parameters of adherent cell surfaces by magnetic bead microrheometry. *Biophys. J.* **75**, 2038–2049.

Butler, J. P. & Kelly, S. M. 1998 A model for cytoplasmic rheology consistent with magnetic twisting cytometry. *Biorheology* **S35**, 193–209.

Chien, S. & Sung, K. L. 1984 Effect of colchicine on viscoelastic properties of neutrophils. *Biophys. J.* **46**, 383–386.

Crick, F. H. C. & Hughes, A. F. W. 1950 The physical properties of cytoplasm. A study by means of the magnetic particle method. *Exper. Cell Res.* **1**, 37–80.

Erdélyi, A., Oberhettinger, M. F. & Tricomi, F. G. 1954 *Tables of integral transformations*. New York: McGraw-Hill.

Evans, E. & Yeung, A. 1989 Apparent viscosity and cortical tension of blood granulocytes determined by micropipet aspiration. *Biophys. J.* **56**, 151–160.

Fabry, B., Maksym, G. N., Butler, J. P., Glogauer, M., Navajas, D. & Fredberg, J. J. 2001 Scaling the microrheology of living cells. *Phys. Rev. Lett.* **87**, 148102.

Fabry, B., Maksym, G. N., Butler, J. P., Glogauer, M., Navajas, D., Taback, N. A., Millet, E. J. & Fredberg, J. J. 2003 Time-scale and other invariants of integrative mechanical behavior in living cells. *Phys. Rev.* E **68**, 041914.

Fielding, S. M., Sollich, P. & Cates, M. E. 2000 Aging and rheology in soft materials. *J. Rheol.* **22**, 323.

Findley, W. N., Lai, J. S. & Onaran, K. 1976 *Creep and relaxation of nonlinear viscoelastic materials with an introduction to linear viscoelasticity*. New York: Dover Publications.

Hu, S., Chen, J., Fabry, B., Numaguchi, Y., Gouldstone, A., Ingber, D. E., Fredberg, J. J., Butler, J. P. & Wang, N. 2003 Intracellular stress tomography reveals stress focusing and structural anisotropy in cytoskeleton of living cells. *Am. J. Physiol. Cell Physiol.* **285**, C1082–C1090.

Hubmayr, R. D., Shore, S. A., Fredberg, J. J., Planus, E., Panettieri, R. A., Jr., Moller, W., Heyder, J. & Wang, N. 1996 Pharmacological activation changes stiffness of cultured human airway smooth muscle cells. *Am. J. Physiol* **271**, C1660–C1668.

Karcher, H., Lammerding, J., Huang, H., Lee, R. T., Kamm, R. D. & Kaazempur-Mofrad, M. R. 2003 A three-dimensional viscoelastic model for cell deformation with experimental verification. *Biophys. J.* **85**(5), 3336–3349.

Koay, E. J., Shieh, A. C. & Athanasiou, K. A. 2003 Creep indentation of single cells. *J. Biomech. Eng.* **125**, 334–341.

Lau, A. W. C., Hoffman, B. D., Davies, A., Crocker, J. C. & Lubensky, T. C. 2003 Microrheology, stress fluctuations, and active behavior of living cells. *Phys. Rev. Lett.* **91**, 198 101–198 104.

Laurent, V. M., Canadas, P., Fodil, R., Planus, E., Asnacios, A., Wendling, S. & Isabey, D. 2002*a* Tensegrity behaviour of cortical and cytosolic cytoskeletal components in twisted living adherent cells. *Acta Biotheor.* **50**, 331–356.

Laurent, V. M., Henon, S., Planus, E., Fodil, R., Balland, M., Isabey, D. & Gallet, F. 2002*b* Assessment of mechanical properties of adherent living cells by bead micromanipulation: comparison of magnetic twisting cytometry vs optical tweezers. *J. Biomech. Eng.* **124**, 408–421.

Mijailovich, S. M., Kojic, M., Zivkovic, M., Fabry, B. & Fredberg, J. J. 2002 A finite element model of cell deformation during magnetic bead twisting. *J. Appl. Physiol.* **93**, 1429–1436.

Puig-De-Morales, M., Millet, E., Fabry, B., Navajas, D., Wang, N., Butler, J. P. & Fredberg, J. J. 2004 Cytoskeletal mechanics in the adherent human airway smooth muscle cell: probe specificity and scaling of protein-protein dynamics. *Am. J. Physiol. Cell. Physiol.* **287**(3), C643–C654.

Segre, P. N., Prasad, V., Schofield, A. B. & Weitz, D. A. 2001 Glass-like kinetic arrest at the colloidal-gelation transition. *Phys. Rev. Lett.* **86**, 6042–6045.

Sollich, P. 1998 Rheological constitutive equation for a model of soft glassy materials. *Phys. Rev.* E **58**, 738–759.

Thoumine, O. & Ott, A. 1997 Time scale dependent viscoelastic and contractile regimes in fibroblasts probed by microplate manipulation. *J. Cell. Sci.* **110**, 2109–2116.

Wang, N., Butler, J. P. & Ingber, D. E. 1993 Mechanotransduction across the cell surface and through the cytoskeleton. *Science* **260**, 1124–1127.

Winter, H. H. & Mours, M. 1997 Rheology of polymers near liquid-solid transitions. *Adv. Polymer Sci.* **134**, 165–234.

Wu, H. W., Kuhn, T. & Moy, V. T. 1998 Mechanical properties of L929 cells measured by atomic force microscopy: effects of anticytoskeletal drugs and membrane crosslinkingT. *Scanning* **20**, 389–397.

Yamada, S., Wirtz, D. & Kuo, S. C. 2000 Mechanics of living cells measured by laser tracking microrheology. *Biophys. J.* **78**, 1736–1747.

Yanai, M., Butler, J. P., Suzuki, T., Sasaki, H. & Higuchi, H. 2004 Regional rheological differences in locomoting neutrophils. *Am. J. Physiol. Cell Physiol.* **287**(3), C603–C611.

Yeung, A. & Evans, E. 1989 Cortical shell-liquid core model for passive flow of liquid-like spherical cells into micropipets. *Biophys. J.* **56**, 139–149.

Ziemann, F., Radler, J. & Sackmann, E. 1994 Local measurements of viscoelastic moduli of entangled actin networks using an oscillating magnetic bead microrheometer. *Biophys. J.* **66**, 2210–2216.